Time-Resolved Detection of the CF_3 Photofragment Using Chirped QCL Radiation

G. Hancock, S. J. Horrocks, G. A. D. Ritchie,* J. H. van Helden, and R. J. Walker

Department of Chemistry, Physical and Theoretical Chemistry Laboratory, The University of Oxford, South Parks Road, Oxford, OX1 3QZ, United Kingdom

Received: June 2, 2008; Revised Manuscript Received: July 16, 2008

This paper demonstrates how a quantum cascade laser (QCL) in its intrapulse mode can provide a simple method for probing the products of a photolysis event. The system studied is the 266 nm photodissociation of CF_3I with the CF_3 fragments subsequently detected using radiation at ~1253 cm^{-1} generated by a pulsed QCL. The tuning range provided by the frequency down-chirp of the QCL operated in its intrapulse mode allows a ~1 cm^{-1} segment of the CF_3 ν_3 band to be measured following each photolysis laser pulse. Identification of features within this spectral region allows the CF_3 ($v = 0$) number density to be calculated as a function of pump−probe delay, and consequently the processes which populate and deplete this quantum state may be examined. Rate constants for the population cascade from higher vibrational levels into the $v = 0$ state, k_1, and for the recombination of the CF_3 radicals to form C_2F_6, k_2, are measured. The returned values of $k_1 = (2.3 \pm 0.34) \times 10^{-12}$ cm^3 $molecule^{-1}$ s^{-1} and $k_2 = (3.9 \pm 0.34) \times 10^{-12}$ cm^3 $molecule^{-1}$ s^{-1} are found to be in good agreement with reported literature values.

Introduction

Within the field of photodissociation studies, a variety of experimental techniques have been employed to probe the resultant photofragments including laser-induced fluorescence, photofragment translational spectroscopy, diode laser FM spectroscopy, and resonance-enhanced multiphoton ionization time-of-flight/velocity-map ion imaging. Although these methods can provide great insight into the details of a dissociation process, they often utilize expensive and specialist equipment and require complex analysis to produce truly quantitative results. The powerful, tuneable mid-infrared radiation generated by a quantum cascade laser (QCL) provides access to a spectral region which is rich in fundamental rovibrational transitions and consequently affords the sensitivity for probing nascent photofragments. Furthermore, the intrapulse mode of the QCL[1,2] is particularly applicable for time-resolved studies of photofragment number densities as a complete spectrum may be measured on a time scale conducive to monitoring both nascent and relaxing fragment concentrations. Although the detection system lacks sub-Doppler resolution, the simplistic and absolute nature of the acquisition process makes QC lasers excellent candidates for postphotolysis kinetic studies.

The photodissociation of CF_3I is an ideal benchmark system to demonstrate the QCL as a probe laser because the photolysis of alkyl iodides and their fluorinated analogues are well-studied processes, mainly due to the convenient energy region in which the first or "A" UV absorption band occurs (210−330 nm).[3−17] Previous investigations of these systems include kinetic studies and quantum yield measurements of the iodine atoms produced[4−6] and direct probing of the dissociation behavior (e.g., excited-state lifetimes and fragment angular distributions) using quantum state specific techniques.[7−13]

The excitation of CF_3I in the A-band results in prompt (~100 fs [10]) and direct dissociation via two decay channels[14,18,19]

$$CF_3I \rightarrow CF_3 + I(^2P_{3/2}) \quad (1)$$

$$CF_3I \rightarrow CF_3 + I^*(^2P_{1/2}) \quad (2)$$

where ($^2P_{3/2}$) and ($^2P_{1/2}$) are the ground, I, and excited spin−orbit state, denoted I*, of the iodine atom, respectively. The I/I* branching ratio is intimately related to the characteristic electronic structure of the A-band that involves promotion of a nonbonding p electron of the iodine atom to an antibonding σ^* molecular orbital, largely involving the C and I atoms.[10] The magnetic circular dichroism experiments of Gedanken and Rowe[20] have shown that this single broadband absorption corresponds to excitation to three dissociative states which, in order of increasing energy, are termed $^3Q_1(E)$, $^3Q_0(A_1)$, and $^1Q_1(E)$, (C_{3V} symmetry), using Mulliken notation.[21] The $^3Q_0 \leftarrow X^1A_1$ transition carries the majority of the oscillator strength near the center of the A-band around 266 nm. The dipole moment for this transition lies parallel to the C−I bond and the subsequent dissociation produces $CF_3 + I^*$. It should be noted that excitation to the $^3Q_0$ state also gives rise to ground state I atoms via nonadiabatic coupling of the $^3Q_0$ and $^1Q_1$ excited surfaces. In contrast to the $^3Q_0 \leftarrow X^1A_1$ transition, the $^1Q_1 \leftarrow X^1A_1$ and $^3Q_1 \leftarrow X^1A_1$ transitions, which possess maxima in the blue (240 nm) and red (300 nm) wings of the A-band respectively, are perpendicular in nature and result in dissociation to produce ground state iodine fragments. Due to the different asymptotic limits and transition polarizations for accessing these states, investigations probing the I/I* branching ratios and the angular distributions of the photofragments can provide direct insight into the trajectories taken on these potential energy surfaces.[8−10,22,23]

The UV photofragmentation of CF_3I has applied interest in a number of areas. First, the iodine atom laser, as first described by Kasper and Pimentel in 1964,[15] uses the photolysis of fluorinated alkyl iodides via the A-band to generate excited iodine atoms ($^2P_{1/2}$), thus providing a population inversion with respect to the ground state ($^2P_{3/2}$). The medium shows transient gain on the corresponding magnetic dipole allowed transition at 1315 nm. In addition, significant interest in the absorption

* To whom correspondence should be addressed. E-mail: ritchie@physchem.ox.ac.uk.

10.1021/jp804849m CCC: $40.75
Published on Web 09/10/2008

and subsequent photodissociation dynamics of CF_3I has been triggered within atmospheric contexts, where CF_3I has been suggested as a possible replacement for CF_3Br, a commonly used chemical fire extinguishing agent.[24] Concerns over atmospheric ozone degradation via catalytic cycles[25,26] lead to a ban on the use of CF_3Br and other brominated gases;[27] however, CF_3I is photolyzed rapidly or is removed through rainout in the lower troposphere so only a tiny fraction of surface CF_3I emissions is predicted to reach the stratosphere. Even so, the potential impact of catalytic cycles involving iodine on stratospheric ozone depletion has ensured that CF_3I photolysis continues to receive significant attention.[3,24,28−31]

Specific interest in the CF_3 radical is found in low-pressure fluorocarbon plasma processing, a key technology in many branches of industry including semiconductor microchip fabrication.[32] The thin fluorinated carbon films deposited with these plasma systems have a low dielectric constant making them applicable for insulating intermediate layers, and thus increasing the performance of the microchips.[33−36] Knowledge of the concentrations and kinetics of the transient reactive species present within plasma is essential for a fundamental understanding of the chemical processes and reactive plasma surface interactions occurring. Although numerous studies have focused on these fluorocarbon plasmas, details of the growth mechanisms for the resultant fluorocarbon films are still not well understood. It is known that the CF, CF_2, and CF_3 radicals play an important role in the etching and deposition process, once formed from dissociation of the feed gas (typically CF_4 or C_4F_8).[37,38] Measurements of the absolute densities of these radicals in the gas phase, which are directly influenced by the surface processes, are therefore key to gaining insight into the growth mechanisms occurring.[39]

In overview, this paper aims to showcase the intrapulse operation mode of a QCL as a novel and relatively simple method for probing the products of a photodissociation event. Specifically, the CF_3 ($v = 0$) fragments from the 266 nm photodissociation of CF_3I are detected using radiation at ∼1253 cm^{-1} generated by a pulsed QCL. The tuning range provided by the frequency down-chirp of the QCL operated in its intrapulse mode allows a ∼1 cm^{-1} segment of the CF_3 ν_3 band to be measured following each photolysis laser pulse. A subsequent kinetic analysis has then enabled a study of the processes which populate and deplete this $v = 0$ quantum state with particular focus on determining the rate constants for the population cascade from higher vibrational levels into the $v = 0$ state, and for the recombination of the CF_3 radicals to form C_2F_6.

Experimental Details

Experiments were carried out in a 50 cm cylindrical glass cell fitted with 50 mm diameter CaF_2 windows, transparent to the counter-propagating UV and 8 μm radiation. The CF_3I [99%, Aldrich] gas flow into the cell was controlled using a needle valve and the pressure was monitored by a capacitance manometer [Ceravac, 0−10 Torr]. The cell was evacuated using a Roots blower backed by a rotary pump [Edwards EH250 and E2M40, respectively].

The CF_3I gas was photolyzed by the frequency quadrupled output of a Nd:YAG laser [Spectra Physics LAB-130]. The 266 nm radiation, produced at an energy of 60 mJ $pulse^{-1}$ when running at 10 Hz, was overlapped with the counter-propagating QCL beam through the use of two custom-made dichroic mirrors [LaserOptik] with high reflectivity (∼84%) for the 266 nm light but high transmission (over 90%) of the 8 μm QCL beam. Once the UV light had passed through the cell, the second dichroic mirror directed the residual radiation into a beam dump to prevent feedback into the QCL system. A quartz flat in front of the beam dump reflected ∼8% of the 266 nm light into a fast photodiode [Hamamatsu S1722−02, 1 ns risetime, spectral range 190−1060 nm] which was used to monitor laser timings.

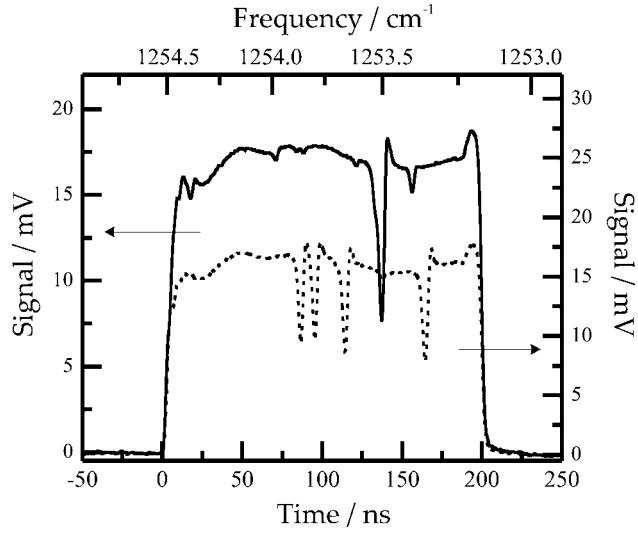

Figure 1. The spectra of N_2O (solid) and CH_4 (dash) used to calibrate the frequency range of the QCL pulse. The spectra are offset for clarity.

The experiments employed a pulsed distributed-feedback QCL (Alpes laser) tuneable between 1248−1257 cm^{-1} through altering the temperature of the laser chip by sending a voltage to a Peltier thermoelectric cooler using a programmable function generator [TTi, Model TG1304]. The laser is housed and driven by a Q-MACS system from Neoplas Control and operates without the need of cryogenic cooling. Laser radiation between 1253.3 − 1254.5 cm^{-1} was created by applying a voltage pulse with a duration of 190 ns to the laser at a chip temperature of −13 °C. This frequency region, not only contains strong CF_3 transitions but also convenient CH_4 and N_2O transitions which can be used to calibrate the frequency chirp of the pulse,[40] as discussed below. Subsequent to exiting the cell, the QCL radiation was collected by an off-axis parabolic mirror and focused onto a thermoelectrically cooled MCT detector [VIGO PCI-2TE-10.6] with a fast preamplifier [Neoplas Control]. The detector was protected from any UV back-reflections by a germanium filter. Signals from the detector were recorded on a 2 Gs/s 350 MHz bandwidth digitizing oscilloscope [LeCroy Wavesurfer 434].

The triggering of the two laser systems and the oscilloscope was achieved using a four-channel digital pulse generator (Stanford Research Systems, Inc.; Model DG 535). This allowed the power of the Nd:YAG laser to be varied by altering the delay between the triggers sent to the flash lamps and Q-switch. Furthermore, the delay between the photolysis pulse (measured by the fast photodiode) and the probe QCL pulse, which was monitored using the oscilloscope, could also be controlled with precision.

The frequency behavior of the QCL pulse was characterized using the CH_4 and N_2O spectra shown in Figure 1. Imperfect impedance matching between the laser and the pulse source causes fluctuations at the beginning of the pulse which limits the useful part of the pulse to frequencies in the range ∼1253.3−1254.2 cm^{-1}. Within this range, the returned relation between frequency and time is almost linear and may be

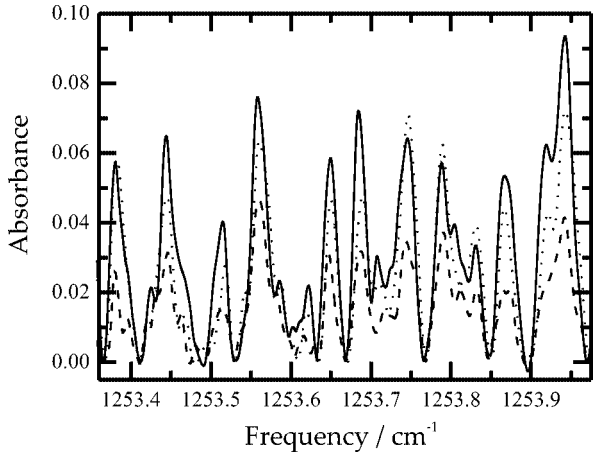

Figure 2. Example CF_3 spectra taken using 4 Torr of CF_3I reactant and a photolysis energy of 29 mJ pulse^{-1}. The traces correspond to different pump−probe delays of 5 (dot), 20 (solid), and 100 μs (dash).

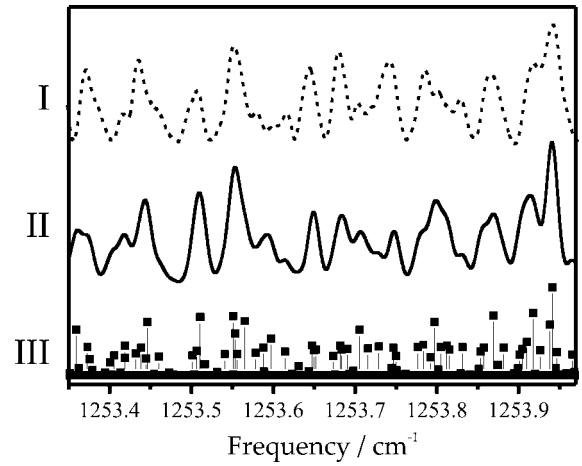

Figure 3. A comparison between the experimental spectrum with 4 Torr of CF_3I and a time delay of 20 μs (I, dash) with those simulated using the Pgopher program with Gaussian widths of 0.015 cm^{-1} (II, solid) and 0.00 cm^{-1} (III, squares).

described by a second order polynomial function which is used to calibrate all spectra taken subsequently onto a frequency scale. The CH_4 and N_2O spectra in Figure 1 are seen to exhibit oscillatory structure, indicating that rapid passage processes are occurring; the rapid chirp rate of the laser (∼200 MHz ns^{-1}) means that the Doppler width of the transition is scanned through on a time scale which is much faster than the relaxation processes present in low-pressure gases.[41] A recent publication has reported the quantification of such effects for our particular laser system.[42]

Results and Discussion

Spectra of the CF_3 produced from CF_3I photodissociation at 266 nm were recorded using five sets of experimental conditions. These conditions relate to two parameters, the pressure of the flowing CF_3I reactant, for which data were taken for 2, 3, and 4 Torr, and the energy of the photolysis laser which was changed from 29 to 20 to 14 mJ pulse^{-1} for the 3 Torr pressure system. For each set of conditions, 10 different pump−probe delays were used, ranging from 2.5 to 500 μs.

The raw signals were seen to be affected by the presence of C_2F_6, which is also a strong absorber in this frequency region (ν_{10} band) and is formed in significant amounts as a result of CF_3 radical recombination. QCL measurements were recorded for a static sample of C_2F_6 within the glass cell at varying pressures in the range 0−170 mTorr. Absorption by C_2F_6 was effectively structureless in this region as a result of spectral congestion. The Beer−Lambert law allows the band strength to be calculated from the QCL measurements for the frequency region 1253.3−1254.2 cm^{-1}, which effectively represents ∼15% of the total band. The value returned for the entire band strength is 1.1 × 10^{-16} cm^2 (cm molecule)$^{-1}$ which is in reasonable agreement with values found previously.[43−47]

A. Spectral Simulation. Knowledge of the expected signal depletion as a result of C_2F_6 absorption allows a background signal, an effective I_0, to be defined for each experimental QCL signal, I. Consequently, the raw QCL spectra can be converted into absorbance signals as a function of frequency, where the absorbance is defined as $-\ln(I/I_0)$. Example spectra are shown in Figure 2 for the 4 Torr pressure system for three different pump−probe delays.

The experimental spectrum for the 20 μs delay case is pictured again in Figure 3 (I) alongside two simulated spectra for the same frequency region (II and III). These simulations were achieved using the Pgopher tool with assistance from Dr Colin Western from the University of Bristol, and using spectral data taken from refs 48 and 49. The full ν_3 band of the CF_3 spectrum is complex and densely packed with spectral lines; the relevant frequency portion of the Pgopher stick spectrum is reproduced in Figure 3 (III) alongside a second spectrum with a Gaussian width of 0.015 cm^{-1} (II), representative of the limited resolution of the QCL, determined by the laser chirp rate and measured in a previous study.[42] The experimental trace (I) shows excellent agreement with the second, broadened Pgopher simulation (II). Since the Pgopher spectrum is simulated for a 300 K sample, the observed agreement with experiment indicates that by 20 μs after photolysis, the CF_3 rotational distribution is approaching that expected for a Boltzmann distribution.

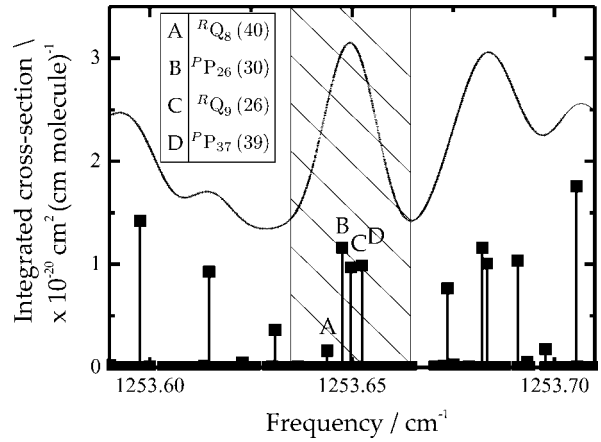

Figure 4. The spectral feature used for the kinetic study is shaded; the stick plot uses data taken from the Pgopher simulation to identify the lines that make up this feature at ∼1253.65 cm^{-1}, as detailed in the key.

B. Kinetic Analysis. To investigate the CF_3 radical kinetics postphotolysis, a specific feature within the recorded spectrum was chosen. This feature, which lies in the frequency range 1253.635−1253.664 cm^{-1}, is highlighted in Figure 4 alongside the Pgopher stick diagram to show its constituent transitions; they have a combined integrated cross-section of 3.28 × 10^{-20} cm^2 (cm molecule)$^{-1}$. By integrating the absorbance in this frequency range for each spectrum, the CF_3 number density in the $v = 0$ quantum state may be calculated as a function of time after photolysis for each set of experimental conditions.

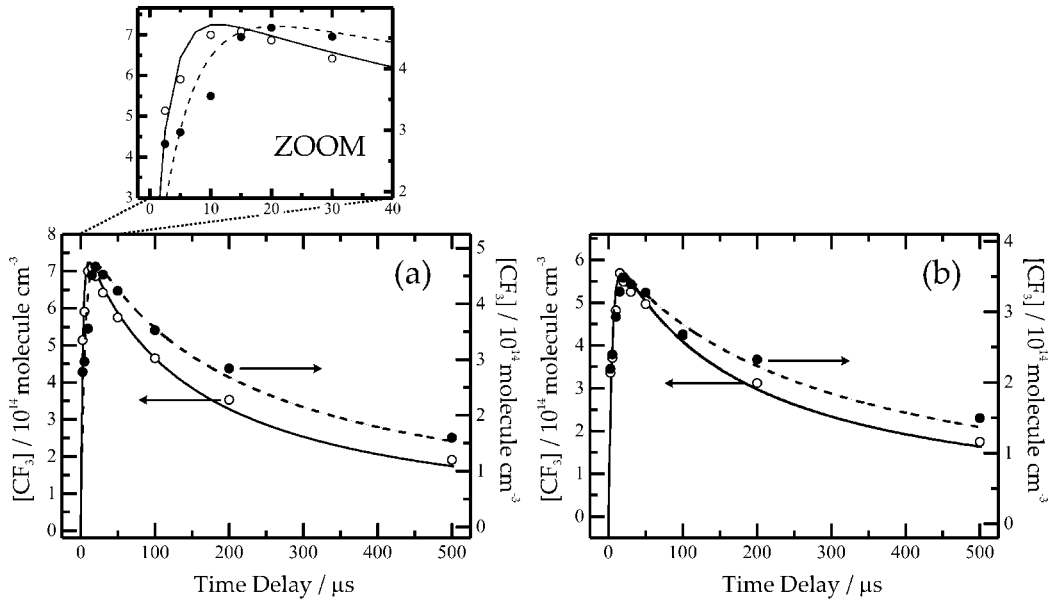

Figure 5. Summary of the extracted CF_3 number densities as a function of pump−probe time delay for two sets of experimental conditions. (a) The effect of increasing CF_3I pressure where the plots refer to 4 Torr (open circle/full line) and 2 Torr (full circle/dash line). (b) The effect of decreasing photolysis power where the plots refer to 29 mJ pulse^{-1} (open circle/full line) and 14 mJ pulse^{-1} (full circle/dash line). The full and dashed lines are fits to the data as explained in the text. We estimate the error in the number density measurements to be 10%.

Figure 5 shows representative results. In Figure 5a data are shown for two total pressures of CF_3I, 2 and 4 Torr at constant laser intensity. At the larger pressure the CF_3 concentration is seen to reach a higher maximum value that at 2 Torr in a slightly shorter time, and then decays more rapidly (the absolute values are scaled to show this effect more clearly). Figure 5b shows data for two laser intensities corresponding to 14 and 29 mJ pulse^{-1} at a total CF_3I pressure of 3 Torr. Here the maximum values of the CF_3 concentrations are seen to increase with laser energy, with the maxima reached in the same times to within experimental error, with a faster decay for the larger CF_3 concentration (larger laser energy).

We interpret the data in terms of the following kinetic scheme for the population and removal of the observed CF_3 ($v = 0$) state, where the rate constants k_1 and k_2 relate to the average vibrational cascade into the $v = 0$ state, and the CF_3 radical−radical recombination process, respectively.

$$CF_3I \rightarrow CF_3\,(v \neq 0) + I \tag{3}$$

$$CF_3\,(v \neq 0) + M \rightarrow M^* + CF_3\,(v = 0) \qquad k_1 \tag{4}$$

$$2CF_3\,(v = 0) \rightarrow C_2F_6 \qquad 2k_2 \tag{5}$$

Here the rate of CF_3 loss by process 5 is described by the kinetic equation

$$-\frac{d[CF_3\,(v=0)]}{dt} = 2k_2[CF_3\,(v=0)]^2 \tag{6}$$

Within this scheme, it is assumed that the initial concentration of CF_3 ($v = 0$) after photolysis is zero. Although this is a simplifying statement, its validity is justified from previous studies investigating the internal energy distribution of the CF_3 fragment following CF_3I dissociation within the A-band.[7−10,14,50] These are discussed briefly here.

Furlan et al.[9] investigated CF_3I photolysis in the wavelength region $\lambda = 275-303$ nm using photofragment translational spectroscopy (PTS). It was found that at 275 nm the proportion of excess energy from the dissociation that was channelled into the internal energy of the CF_3 fragment was 15 and 17% for the I* and I channels, respectively. These findings are corroborated by the work of Felder et al.[7,8] who found that the fraction of available energy channelled into CF_3 internal excitation rises from 15 to 23% between 308 and 248 nm for the I channel, and 5 to 26%, over the same wavelength region, for the I* channel. In addition, in a diode laser gain FM study by Hancock et al.[10] it was reported that 17% of the available energy is channelled into CF_3 fragment internal modes at 266 nm. Although a partitioning of the internal energy into rotational and vibrational contributions cannot be derived from these data, the rotational contribution is expected to be small since the separation of the iodine atom and the CF_3 moiety proceeds predominantly along the 3-fold molecular symmetry axis.[14,51] This hypothesis is in agreement with the observed vibrational resolution in the PTS experiments of Wang et al.[50] and Felder et al.,[7,8] which imply minimal rotational excitation in the CF_3 product. Wang et al.[50] found following CF_3I photolysis at 248 nm that the photofragment translational spectra of the I* revealed 8 well-resolved vibrational peaks where the highest peak was assigned to $v = 5$ of the ν_2 "umbrella" vibrational mode, which has a vibrational frequency of 703 cm^{-1}.[7] In this study, only 1% of the population was found in the $v = 0$ level. These findings are in broad agreement with the CF_3 vibrational populations measured by van Veen et al.,[14] again following photolysis of CF_3I at 248 nm. The vibrational distribution was found to peak at $v = 6$ and to have appreciable population up until $v = 16$. Of specific interest here, the population in the $v = 0$ level was reported as only 8% that of the most populated level.

In summary, between 15−25% of the available energy after dissociation within the A-band is channelled into vibrational excitation in the CF_3 fragment leading to significant population in a number of vibrational states. In particular, for the I* channel following the dissociation of CF_3I at 266 nm, of the ∼11200 cm^{-1} of energy available following dissociation, it is estimated that approximately 2500 cm^{-1} is channelled into CF_3 vibrations,[7] suggesting appreciable population in excited vibrational states, in agreement with the studies carried out at 248 nm.[7,14,50] In

TABLE 1: Experimental Conditions for Variation of [CF_3 ($v = 0$)] with Laser Energy and Total Pressure, Together with the Initial [CF_3 ($v \neq 0$)]$_0$ Concentrations and the Fitted k_1 and k_2 Rate Constants for the Vibrational Cascade into the $v = 0$ State and the Radical−Radical Recombination Process, respectively[a]

				without rapid passage effects		with rapid passage effects	
expt No.	p(CF_3I) (Torr)	photolysis energy (mJ pulse^{-1})	[CF_3 ($v \neq 0$)]$_0$ (molecule cm^{-3})	$k_1 \pm 2\sigma$ (cm^3 molecule^{-1} s^{-1})	$k_2 \pm 2\sigma$ (cm^3 molecule^{-1} s^{-1})	$k_1 \pm 2\sigma$ (cm^3 molecule^{-1} s^{-1})	$k_2 \pm 2\sigma$ (cm^3 molecule^{-1} s^{-1})
1	4	29	7.72×10^{14}	$(2.89 \pm 0.68) \times 10^{-12}$	$(4.51 \pm 0.44) \times 10^{-12}$	$(2.43 \pm 0.34) \times 10^{-12}$	$(3.78 \pm 0.34) \times 10^{-12}$
2	3	29	6.26×10^{14}	$(2.17 \pm 0.68) \times 10^{-12}$	$(4.61 \pm 0.44) \times 10^{-12}$	$(2.21 \pm 0.34) \times 10^{-12}$	$(4.01 \pm 0.34) \times 10^{-12}$
3	2	29	5.02×10^{14}	$(2.93 \pm 0.68) \times 10^{-12}$	$(4.57 \pm 0.44) \times 10^{-12}$	$(2.54 \pm 0.34) \times 10^{-12}$	$(3.92 \pm 0.34) \times 10^{-12}$
4	3	20	4.72×10^{14}	$(2.14 \pm 0.68) \times 10^{-12}$	$(4.07 \pm 0.44) \times 10^{-12}$	$(2.05 \pm 0.34) \times 10^{-12}$	$(3.68 \pm 0.34) \times 10^{-12}$
5	3	14	3.44×10^{14}	$(2.44 \pm 0.68) \times 10^{-12}$	$(4.70 \pm 0.44) \times 10^{-12}$	$(2.32 \pm 0.34) \times 10^{-12}$	$(4.17 \pm 0.34) \times 10^{-12}$

[a] Values are shown when the number densities have and have not been corrected for the effects of rapid passage.

light of this, the initial concentration in the $v = 0$ quantum state is taken to be zero within the kinetic model for the CF_3 fragment.

A second assumption that is made within the kinetic scheme is the preferential relaxation of the vibrationally excited CF_3, over recombination to form excited C_2F_6, which then itself relaxes. This assumption may be justified on two fronts. First, due to the relative concentrations of parent gas molecules compared with CF_3* radicals, the likelihood that an excited CF_3 radical will encounter a buffer gas molecule is far higher than collision with a second CF_3*. In addition, whenever two CF_3* species do collide the excited state complex C_2F_6* formed will be more difficult to stabilize through collisions than that formed from the coming together of two ground state species. Further, work by Smith et al.[52] highlights the fact that when both colliding species are radicals, there is convincing evidence that relaxation can occur *v*ia collision complex formation. This mechanism greatly facilitates vibrational energy transfer so that even when two CF_3* species do collide, it is likely that following complex formation, vibrational relaxation of one of the radicals will occur in preference to relaxation of the C_2F_6* molecule.[52]

From the kinetic scheme detailed previously, the rates of change of the CF_3 ($v \neq 0$) and CF_3 ($v = 0$) concentrations are given by the following differential equations

$$\frac{d[CF_3\ (v \neq 0)]}{dt} = -k_1 M[CF_3\ (v \neq 0)] \tag{7}$$

$$\frac{d[CF_3\ (v = 0)]}{dt} = k_1 M[CF_3\ (v \neq 0)] - 2k_2[CF_3\ (v = 0)]^2 \tag{8}$$

and the solutions to these equations are thus

$$[CF_3\ (v \neq 0)](t) = [CF_3\ (v \neq 0)]_0 e^{-k_1 M t} \tag{9}$$

$$[CF_3\ (v = 0)](t) = \boldsymbol{R}\left(\frac{(k_1 M[CF_3\ (v \neq 0)]_0)^{1/2} e^{-\frac{1}{2}k_1 M t}\left(i\mathrm{BY}_1 - \frac{i\mathrm{BY}_2\mathrm{BY}_1}{\mathrm{BI}_2}\right)}{(2k_2)^{1/2}\left(\frac{i\mathrm{BY}_2\mathrm{BI}_3}{\mathrm{BI}_2} + \mathrm{BY}_1\right)}\right) \tag{10}$$

In eq 10, the BI and BY functions are Bessel functions of the first and second kind, respectively, as defined in the Appendix. The parameter M relates to the buffer gas pressure, taken to be the pressure of CF_3I reactant gas flowing. [CF_3 ($v \neq 0$)] is the initial number of CF_3 molecules produced from the photolysis pulse, which was estimated for each experiment from the measured number of UV photons absorbed. The experimental kinetic traces shown in Figure 5 were then fitted by optimizing the values of k_1 and k_2 using the least-squares fit tool in MATLAB. The initial [CF_3 ($v \neq 0$)] inputs for the fitting program are listed in Table 1 for each set of experimental conditions, numbered 1−5. Examples of the fitted plots are also presented in Figure 5 with the extracted rate constants listed in Table 1. The fitted data show good consistency in the values of k_1 and k_2, with identification of the rising and falling rates as relaxation and recombination, respectively.

The CF_3 spectra are, as mentioned previously, complex in nature and densely packed with spectral features and as a result, they lack any appearance of the rapid passage signals which were evident in the N_2O and CH_4 spectra shown in Figure 1. In a previous publication, an investigation was carried out which examined rapid passage signals in methane spectra and demonstrated how the resulting oscillatory structure can be quenched through buffering.[42] It was observed that 100 mTorr of methane required ~30 Torr of N_2 buffer to return the spectral line shape to a Voigt profile, and when 5 Torr of buffer was used, the measured density was ~90% of that expected. Work by Duxbury and co-workers[53] has highlighted that rapid passage signals depend upon numerous factors including the interaction path length, the strength of the transition under study, the laser power and its chirp rate. Although the influence of rapid passage is not observed in the CF_3 spectra shown here, the effects of rapid passage on the number densities should still be accounted for. The measurements carried out previously[42] focused on transitions of a similar strength to the combined line strength of the spectral feature examined here. Furthermore, the laser system is the same and interaction path length comparable for the two experiments. Consequently, it would seem reasonable to assume a similar correction factor of 10% should be employed to the CF_3 number densities, present in ~5 Torr of bath gas. Fitting the resultant, corrected number densities returns rate constants which are also listed in Table 1. For both k_1 and k_2, the determined values are not seen to change within the statistical error limits with inclusion of the correction factor, and we report values of $k_1 = (2.3 \pm 0.34) \times 10^{-12}$ cm^3 molecule^{-1} s^{-1} and $k_2 = (3.9 \pm 0.34) \times 10^{-12}$ cm^3 molecule^{-1} s^{-1}; errors represent 2σ of the average of the values reported in Table 1.

The kinetics of the $CF_3 + CF_3 \rightarrow C_2F_6$ recombination reaction have been extensively studied by various research groups.[54−60] The recombination rate constants, k_2, which have been measured at different temperatures and for different pressure regimes, fall within a relatively wide range from 2×10^{-12} to 40×10^{-12} cm^3 molecule^{-1} s^{-1}. Example studies within a similar pressure regime and 300 K have been carried out by Brown et al.[58] and Vakhtin[60] who reported rate constants of 2.2×10^{-12} and 3.9×10^{-12} cm^3 molecule^{-1} s^{-1}, respectively. These results are shown together with the present data in Figure 6. The calculated

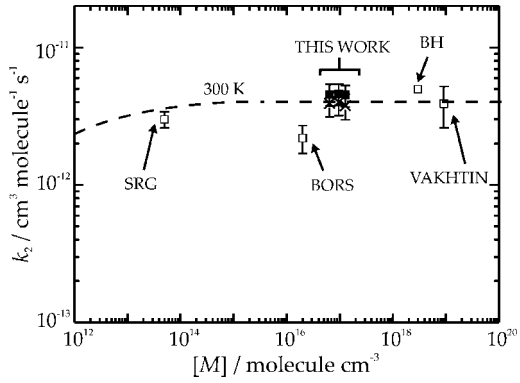

Figure 6. Example experimental k_2 values obtained at 300 K (open square); BH,[54] SRG,[57] BORS,[58] VAKHTIN.[60] Also shown is the calculated falloff curve $k_2([M])$, M = He for 300 K. The crosses and closed squares are the k_2 values from this work, determined with and without rapid passage effects being accounted for, respectively.

falloff curve,[60] also shown in Figure 6, was made for He as the buffer gas and implies that under our conditions the limiting high pressure rate constant has been reached, consistent with the returned constant value of k_2 found over the relatively small pressure range of 2−4 Torr CF_3I. Error sources may include the fact that CF_3 loss processes including diffusion out of the probe beam profile and wall collisions are neglected, as are longitudinal variation of $[CF_3]_0$ from photolysis along the beam path. In addition, the influence of rapid passage on the returned number densities has only been estimated.

Within this study, state-specific information about the vibrational cascade into the $v = 0$ level is not obtained, and we cannot unravel the exact details of the relaxation process. The simple analysis presented gives only a useful phenomenological rate constant falling in the range $(2-3) \times 10^{-12}$ cm^3 molecule^{-1} s^{-1}. An indirect study investigating the vibrational relaxation of the CF_3 radical has been carried out by Young and Pimentel[61] in their investigation into the chemical effects of CF_3 vibrational energy content on the abstraction reaction $CF_3 + Br_2 \rightarrow CF_3Br + Br$. Within this work, a relaxation rate was determined for vibrationally hot CF_3, buffered with 25 Torr of CO_2 with a returned rate constant of 1.08×10^{-12} cm^3 molecule^{-1} s^{-1}, in reasonable agreement with the values reported here.

Summary

The work presented in this study has demonstrated the intrapulse operation mode of quantum cascade lasers as an effective and simple method for probing the products of a photodissociation event. For the photolysis of CF_3I at 266 nm, rate constants have been extracted for the recombination of the CF_3 radical fragments to form C_2F_6, and for the average vibrational cascade into the ground state vibrational level, these are in good agreement with literature values.

Acknowledgment. The authors gratefully acknowledge the Royal Society for the award of a Royal Society University Research Fellowship to G.A.D.R, the EPSRC for the research grant and studentship for R.J.W., and NERC for a studentship for S.J.H. S.J.H. would also like to thank the George Drexler Foundation for their support. We also would like to thank Dr. Colin Western for helpful discussions regarding the simulation of the CF_3 spectrum.

Appendix

The Bessel Functions used in the Kinetic Model of CF_3 are

$$i\mathrm{BY}_1 = i\mathrm{BesselY}\left(1, \left(\frac{2\sqrt{2}ik_2^{1/2}[\mathrm{CF}_3\,(v\neq 0)]^{1/2}e^{-1/2k_1Mt}}{k_1^{1/2}M^{1/2}}\right)\right) \quad \text{(A.1)}$$

$$i\mathrm{BY}_2 = i\mathrm{BesselY}\left(1, \left(\frac{2i\sqrt{2}k_2^{1/2}[\mathrm{CF}_3\,(v\neq 0)]^{1/2}}{k_1^{1/2}M^{1/2}}\right)\right) \quad \text{(A.2)}$$

$$\mathrm{BI}_1 = \mathrm{BesselI}\left(1, \left(\frac{2\sqrt{2}k_2^{1/2}[\mathrm{CF}_3\,(v\neq 0)]^{1/2}e^{-1/2k_1Mt}}{k_1^{1/2}M^{1/2}}\right)\right) \quad \text{(A.3)}$$

$$\mathrm{BI}_2 = \mathrm{BesselI}\left(1, \left(\frac{2\sqrt{2}k_2^{1/2}[\mathrm{CF}_3\,(v\neq 0)]^{1/2}}{k_1^{1/2}M^{1/2}}\right)\right) \quad \text{(A.4)}$$

$$\mathrm{BI}_3 = \mathrm{BesselI}\left(0, \left(\frac{2\sqrt{2}k_2^{1/2}[\mathrm{CF}_3\,(v\neq 0)]^{1/2}e^{-1/2k_1Mt}}{k_1^{1/2}M^{1/2}}\right)\right) \quad \text{(A.5)}$$

$$BY_1 = BesselY\left(0, \left(\frac{2\sqrt{2}ik_2^{1/2}[\mathrm{CF}_3\,(v\neq 0)]^{1/2}e^{-1/2k_1Mt}}{k_1^{1/2}M^{1/2}}\right)\right) \quad \text{(A.6)}$$

The parameters M and $[CF_3\,(v \neq 0)]$ relate to the pressure of the buffer gas (taken to be the pressure of the flowing CF_3I gas), and the initial number of CF_3 molecules produced from the photolysis pulse.

References and Notes

(1) Beyer, T.; Braun, M.; Lambrecht, A. *J. Appl. Phys.* **2003**, *93*, 3158.
(2) McCulloch, M. T.; Normand, E. L.; Langford, N.; Duxbury, G.; Newnham, D. A. *J. Opt. Soc. Am. B* **2003**, *20*, 1761.
(3) Fahr, A.; Nayak, A. K.; Huie, R. E. *Chem. Phys.* **1995**, *199*, 275.
(4) Baklanov, A. V.; Aldener, M.; Lindgren, B.; Sassenberg, U. *Chem. Phys. Lett.* **2000**, *325*, 399.
(5) Kavita, K.; Das, P. K. *J. Chem. Phys.* **2002**, *117*, 2038.
(6) Hess, W. P.; Kohler, S. J.; Haugen, H. K.; Leone, S. R. *J. Chem. Phys.* **1986**, *84*, 2143.
(7) Felder, P. *Chem. Phys.* **1990**, *143*, 141.
(8) Felder, P.; Haas, B. M.; Huber, J. R. *Chem. Phys. Lett.* **1991**, *186*, 177.
(9) Furlan, A.; Gejo, T.; Huber, J. R. *J. Phys. Chem.* **1996**, *100*, 7956.
(10) Hancock, G.; Hutchinson, A.; Peverall, R.; Richmond, G.; Ritchie, G. A. D.; Taylor, S. *Phys. Chem. Chem. Phys.* **2007**, *9*, 2234.
(11) Tian, Z.; Bi, W.; Deng, H.; Wang, X.; Tang, Z.; Zhu, Q. *Chem. Phys. Lett.* **2004**, *400*, 15.
(12) Kavita, K.; Das, P. K. *Chem. Phys. Lett.* **2001**, *338*, 118.
(13) Eppink, A. T. J. B.; Parker, D. H. *J. Chem. Phys.* **1998**, *109*, 4758.
(14) van Veen, G. N. A.; Baller, T.; de Vries, A. D.; Shapiro, M. *Chem. Phys.* **1985**, *93*, 277.
(15) Kaspar, J. V. V.; Pimental, G. C. *Appl. Phys. Lett.* **1964**, *5*, 231.
(16) He, Y. B.; Pochert, J.; Quack, M.; Ranz, R.; Seyfang, G. *Faraday Discuss.* **1995**, *102*, 275.
(17) Brewer, P.; Das, P.; Ondrey, G.; Bersohn, R. *J. Chem. Phys.* **1983**, *79*, 720.
(18) Clary, D. C. *J. Chem. Phys.* **1986**, *84*, 4288.
(19) Untch, A.; Hannig, S.; Schinke, R. *Chem. Phys.* **1988**, *126*, 181.
(20) Gedanken, A.; Rowe, M. D. *Chem. Phys. Lett.* **1975**, *34*, 39.
(21) Mulliken, R. *Phys. Rev.* **1936**, *50*, 1017.
(22) Aguirre, F.; Pratt, A. T. *J. Chem. Phys.* **2002**, *118*, 1175.
(23) Kim, Y. S.; Kang, W. K.; Jung, K.-H. *J. Chem. Phys.* **1996**, *105*, 551.
(24) Li, Y.; Wuebbles, D. J. *Atmos. Chem. and Phys. Disc.* **2006**, *6*, 5163.
(25) Solomon, S. *Nature* **1990**, *347*, 347.

(26) Brune, W. H.; Anderson, J. G.; Tooley, D. W.; Farley, D. W.; Kawa, S. R.; Jones, R. L.; McKenna, D. S.; Poole, L. R. *Science* **1991**, *252*, 1260.

(27) Abstract, Copenhagen Amendment to the Montreal Protocol on Substances that deplete the Ozone Layer, Copenhagen, December 7th, 1992, United Nations Environments Programme (UNEP) Ozone Secretariat, UNEP, Nairoibi, Kenya.

(28) Gilles, M. K.; Talukdar, R. K.; Ravishankara, A. R. *J. Phys. Chem. A* **2000**, *104*, 8945.

(29) Solomon, S.; Garcia, R. R.; Ravishankara, A. R. *J. Geophys. Res.* **1994**, *99*, 20491.

(30) Solomon, S.; Burkholder, J. B.; Garcia, R. R.; Ravishankara, A. R. *J. Geophys. Res.* **1994**, *99*, 20929.

(31) Saiz-Lopez, A.; Saunders, R. W.; Joseph, D. M.; Ashworth, S. H.; Plane, J. M. C. *Atmos. Chem. Phys.* **2004**, *4*, 1443.

(32) Tachi, S. *J. Vac. Sci. Technol., A* **2003**, *21*, 131.

(33) Theil, J. A. *J. Vac. Sci. Technol., B* **1999**, *17*, 2397.

(34) Capps, N. E.; Mackie, N. M.; Fisher, E. R. *J. Appl. Phys.* **1998**, *84*, 4736.

(35) Endo, K.; Tatsumi, T. *Appl. Phys. Lett.* **1996**, *68*, 2864.

(36) Gabriel, O.; Stepanov, S.; Pfafferott, M.; Meichsner, J. *Plasma Sources Sci. Technol.* **2006**, *15*, 858.

(37) Inayoshi, M.; Ito, M.; Hori, M.; Goto, T.; Hiramatsu, M. *J. Vac. Sci. Technol., A* **1998**, *16*, 233.

(38) Goto, T.; Hori, M. *J. Appl. Phys.* **1996**, *35*, 6521.

(39) Hori, M.; Goto, T. *Plasma Sources Sci. Technol.* **2006**, *15*, S74.

(40) Rothman, L. S.; Jacquemart, D.; Barbe, A.; Benner, D. C.; Birk, M.; Brown, L. R.; Carleer, M. R.; Chackerian, C., Jr.; Chancea, K.; Coudert, L. H.; Dana, V.; Devi, V. M.; Flaud, J.-M.; Gamache, R. R.; Goldman, A.; Hartman, J.-M.; Jucks, K. W.; Maki, A. G.; Mandin, J.-Y.; Massie, S. T.; Orphal, J.; Perrin, A.; Rinsland, C. P.; Smith, M. A. H.; Tennyson, J.; Tolchenov, R. N.; Toth, R. A.; van der Auwera, J.; Varanasi, P.; Wagner, G. *J. Quant. Spectrosc. Radiat. Transfer* **2005**, *96*, 139.

(41) McCulloch, M. T.; Duxbury, G.; Langford, N. *Mol. Phys.* **2006**, *104*, 2767.

(42) van Helden, J. H.; Horrocks, S. J.; Ritchie, G. A. D. *Appl. Phys. Lett.* **2008**, *92*, 081506.

(43) Zou, Q.; Sun, C.; Nemtchinov, V.; Varanasi, P. *J. Quant. Spectrosc. and Radiat. Transfer.* **2004**, *83*, 215.

(44) Roehl, C. M.; Boglu, D.; Bruhl, C.; Moortgat, G. K. *Geophys. Rev. Lett.* **1995**, *22*, 815.

(45) Varanasi, P.; Chudamani, S. *J. Geophys. Res.* **1988**, *93*, 851.

(46) Olliff, M. P.; Fisher, G. *Spectrochim. Acta* **1994**, *50*A, 2223.

(47) Mills, I. M.; Person, W. B.; Scherer, J. R.; Crawford, B., Jr. *J. Chem. Phys.* **1958**, *28*, 851.

(48) Yamada, C.; Hirota, E. *J. Chem. Phys.* **1983**, *78*, 1703.

(49) Orlando, J. J.; Smith, D. R. *J. Phys. Chem.* **1988**, *92*, 5147.

(50) Wang, X.; Tian, Z.; Shi, T.; Shi, X.; Yang, D.; Zhu, Q. *Chem. Phys. Lett.* **2003**, *380*, 600.

(51) Hannig, S.; Engel, V.; Schinke, R. *J. Chem. Phys.* **1986**, *84*, 5444.

(52) Smith, I. W. M.; Williams, M. D. *J. Chem. Soc., Faraday. Trans.* **1985**, *81*, 1849.

(53) Duxbury, G.; Langford, N.; McCulloch, M. T.; Wright, S. *Chem. Soc. Rev.* **2005**, *34*, 921.

(54) Basco, N.; Hathorn, F. G. M. *Chem. Phys. Lett.* **1971**, *8*, 291.

(55) Rossi, M.; Golden, D. M. *Int. J. Chem. Kinet.* **1979**, *11*, 775.

(56) Glanzer, K.; Maier, M.; Troe, J. *J. Phys. Chem.* **1980**, *84*, 1681.

(57) Selarnoglu, N.; Rossi, M. J.; Golden, D. M. *Chem. Phys. Lett.* **1986**, *124*, 68.

(58) Brown, C. E.; Orlando, J. J.; Reid, J.; Smith, D. R. *Chem. Phys. Lett.* **1987**, *142*, 213.

(59) Robertson, R. M.; Golden, D. M.; Rossi, M. J. *J. Phys. Chem.* **1988**, *92*, 5338.

(60) Vakhtin, A. B. *Int. J. Chem. Kin.* **1996**, *28*, 443.

(61) Young, M. A.; Pimental, G. C. *Int. J. Chem. Kin.* **1991**, *23*, 57.

JP804849M